CrossMark

RESEARCH PAPER

Synthesis of Titanium-doped MgO heteronanostructures with tunable band gap

Urvashi Sharma · P. Jeevanandam

Abstract $Ti_xMg_{1-x}O$ heteronanostructures ($x = 0.02$ to 0.50) have been synthesized by a novel thermal decomposition route, and the effect of concentration of titanium and calcination temperature on optical properties of the heteronanostructures has been investigated. Phase analysis using powder X-ray diffraction demonstrates the formation of mixture of MgO and $MgTiO_3$ when $x = 0.02$ to 0.20 and pure $MgTiO_3$ when $x = 0.33$ to 0.50. Scanning electron microscopy studies show that the $Ti_xMg_{1-x}O$ samples with $x = 0.02$ to 0.20 consist of particles with a mixture of flower- and rod-like morphology, whereas the $Ti_xMg_{1-x}O$ samples with $x = 0.33$ to 0.50 possess rod-like morphology. Transmission electron microscopy studies show that the flowers are in turn formed by assembly of nanoparticles and the hollow rods are formed by aggregation of dumbbell-shaped nanoparticles. Diffuse reflectance spectroscopic studies show that band gap of the $Ti_xMg_{1-x}O$ heteronanostructures can be tuned from 3.2 to 4.2 eV by varying the concentration of titanium and the calcination temperature. Photoluminescence spectra show emission bands in visible and near-infrared regions due to defects present in the $Ti_xMg_{1-x}O$ heteronanostructures.

U. Sharma · P. Jeevanandam (✉)
Department of Chemistry, Indian Institute of Technology Roorkee, Roorkee 247667, India
e-mail: jeevafcy@iitr.ernet.in;
jeevafcy@iitr.ac.in

Introduction

Magnesium oxide is widely used for various applications as it is chemically stable (Gao et al. 2012). The electrical resistance of MgO is high and it is a promising material for high-temperature insulation (Ceylantekin and Aksel 2012). MgO has been used as an adsorbent (Bian et al. 2010; Dadvar et al. 2013; Tian et al. 2013), bactericide (Rao et al. 2013), and a catalyst (Bain et al. 2008). TiO_2 is an n-type semiconductor and it is used in a variety of applications such as photocatalysis (Wang et al. 2004), lithium-ion batteries (Jiang et al. 2012; Li et al. 2012), water splitting (Liu et al. 2011), and dye-sensitized solar cells (Cheng et al. 2013; Qu et al. 2010; Zhang et al. 2014). When MgO and TiO_2 co-exist, the mixed phase collectively exhibits unique properties and binary $MgO–TiO_2$ systems have been widely investigated due to their applications in photocatalysis (Bandara et al. 2004, 2006), dielectrics (Tang et al. 2014; Xue et al. 2013), and dye-sensitized solar cells (Jung et al. 2005; Li et al. 2011).

In general, when trace amount of a cation is added to a pure metal oxide, doping of the cation in the host metal oxide takes place. Up to about 4 % titanium ions

can be incorporated into MgO lattice as it is the maximum solubility of titanium in MgO (Wang et al. 2008). Doping of Ti^{4+} ions in MgO generates defects that affect nature of the grain boundaries and causes n-type conductivity (Lee and Ko 2014). Different synthetic routes have been reported for the synthesis of Ti^{4+}-doped MgO and MgO–TiO_2 mixed metal oxides such as sol–gel method (Rao et al. 2013; Bokhimi et al. 1999), co-precipitation (Wang et al. 2008, 2009), and solid-state reaction (Yang and Shen 2005). The most stable phases in which Mg^{2+} and Ti^{4+} ions co-exist are Mg_2TiO_4, $MgTiO_3$, and $MgTi_2O_5$ and their bulk band gap values are 3.6 eV, 3.7 eV, and 3.4 eV, respectively (Ho et al. 2014; Qu et al. 2013; Pfaff 1994). Among these three phases, $MgTiO_3$ has been widely investigated for various applications such as dilute magnetic semiconductors (Fujioka et al. 2011, 2012), photocatalysis (Qu et al. 2013; Shrestha et al. 2013), and dielectric materials (Tang et al. 2014; Gao et al. 2008; Huang et al. 2011). A number of synthetic methods have been reported for the synthesis of $MgTiO_3$ such as solid-state reaction (Fujioka et al. 2011; Tang et al. 2014; Huang et al. 2011), thermal decomposition of precursors (Qu et al. 2013), hydrothermal synthesis (Dong et al. 2011), and sol–gel method (Mohammadi and Fray 2012).

Ethylene glycol is a reducing solvent with high boiling point ($\sim$197 °C) and the synthesis of materials based on ethylene glycol is called polyol synthesis. Metal ions form alkoxides on reaction with ethylene glycol, and the alkoxide species assemble to form metal glycolates with different morphologies (Chakroune et al. 2005) and different metal ions show different behavior. For example, on reaction with ethylene glycol, metals such as magnesium and nickel form layered glycolates, whereas titanium forms linear chains (Chakroune et al. 2005; Pol et al. 2007). The morphologies reported for the metal oxides synthesized using glycolate precursors include nanoflowers, nanorods, spheres, multi-faceted structures, nanoneedles, nanowires, nanopillars, and nanodisks (Bain et al. 2008; Wang et al. 2004; Jiang et al. 2012; Li et al. 2012; Liu et al. 2011; Qu et al. 2010; Zhang et al. 2014; Cheng et al. 2013; Qu et al. 2013; Chakroune et al. 2005; Cao et al. 2006; Wang et al. 2015; Qu et al. 2012).

Bain et al. have reported the synthesis of coralline MgO via glycolate precursor (Bain et al. 2008). Qu et al. and Wang et al. have reported the synthesis of $MgTiO_3$–$MgTi_2O_5$ heterogeneous and mesoporous nanorods by an ethylene glycol-mediated route at room temperature, respectively (Qu et al. 2013; Wang et al. 2015). Chakroune et al. have reported the formation of disk-shaped cobalt oxide nanostructures via cobalt glycolate (Chakroune et al. 2005) and Cao et al. have reported the synthesis of hierarchically structured cobalt oxide nanoparticles using glycolate precursors (Cao et al. 2006). Yadav et al. have studied the synthesis of bi- and tri-metallic titanium-based oxides with rod-like morphology via glycolate precursors (Yadav et al. 2011). Qu et al. have reported the synthesis of $NiTiO_3$ nanorods via metal glycolate precursors (Qu et al. 2012) and Subramania et al. have reported the synthesis of MgO nanowires via polyol process (Subramania et al. 2007). The present study reports the synthesis and band gap tuning of morphologically interesting MgO–$MgTiO_3$ and $MgTiO_3$ heteronanostructures in a wide range (3.2–4.2 eV). Although ethylene glycol-mediated route has been reported for the synthesis of various metal glycolates, the synthesis of band gap (3.2–4.2 eV)-tunable Ti^{4+}-doped MgO heteronanostructures from Ti–Mg glycolates with a wide range of titanium concentration (0.02–0.50 mmol) and with a mixture of flower- and hexagonal rod-like morphology has been reported for the first time.

In the present study, $Ti_xMg_{1-x}O$ samples with $x = 0.02$–0.50 have been synthesized by the thermal decomposition of Ti–Mg glycolate precursors (Bain et al. 2008). Titanium isopropoxide and magnesium acetate with different molar ratios were thermally decomposed in ethylene glycol in the presence of poly(vinylpyrrolidone) (PVP) to obtain metal glycolate precursors. The precursors were calcined at 500 and 700 °C to obtain a mixture of MgO and $MgTiO_3$ when $x = 0.02$–0.20 and pure $MgTiO_3$ is formed when $x = 0.33$–0.50. Thermal stability of the Ti–Mg glycolate precursors was investigated by thermogravimetric analysis and functional group analysis was carried out using IR spectroscopy. Phase analysis of the $Ti_xMg_{1-x}O$ samples was carried out using powder X-ray diffraction, morphological properties were studied by FE-SEM and TEM analysis, and optical properties of the $Ti_xMg_{1-x}O$ samples were investigated by diffuse reflectance spectroscopy and photoluminescence spectroscopy.

Experimental procedure

Materials

The chemicals used for the synthesis of Ti–Mg glycolates were magnesium acetate tetrahydrate (Himedia, 98 %), titanium isopropoxide (Aldrich, 97 %), ethylene glycol (Rankem®, 98 %), poly(vinylpyrrolidone)-10 (Aldrich), and ethanol (Changshu Yangyuan Chemical, China, AR, 99.9 %). All the chemicals were used as received.

Synthesis

Thermal decomposition method was used to prepare the Ti–Mg glycolates (Bain et al. 2008). Titanium isopropoxide and magnesium acetate were taken in different molar ratios (titanium isopropoxide: magnesium acetate = 0:1.0, 0.02:0.98, 0.04:0.96, 0.10:0.90, 0.20:0.80, 0.33:0.66, 0.50:0.50, and 1.0:0) and the total concentration of the reagents was kept constant (1 mmol). The contents were thermally decomposed in ethylene glycol (20 mL) at 180 °C for about 150 min in the presence of 1.5 mmol (166 mg) of poly(vinylpyrrolidone). A white product was formed in each reaction which was washed three times with ethanol and dried overnight in an oven at about 80 °C. The obtained Ti–Mg glycolates were calcined at 500 and 700 °C for 2 h with a heating rate of 2 °C per minute in a muffle furnace (Nabertherm®). The designation of $Ti_xMg_{1-x}O$ samples along with the concentration of the reagents used is given in Table 1 and the calcination temperature is mentioned along with the sample ID. For example, the Ti^{4+}-doped MgO sample, prepared using 0.02 mmol of titanium isopropoxide and 0.98 mmol of magnesium acetate and calcined at 500 °C, is designated as [Ti:Mg = 0.02:0.98]-500.

Characterization

Phase analysis was carried out using a Bruker AXS D8 Advance powder X-ray diffractometer with Cu-Kα radiation ($\lambda = 1.5406$ Å) and scan speed, 1˚/min. Thermo-gravimetric analysis was carried out using a Perkin Elmer Pyris Diamond instrument and the Ti–Mg glycolates were heated from 30 to 1000 °C with a heating rate of 10 °C min^{-1} in air. Infrared spectra of the Ti–Mg glycolates were recorded using a Thermo Nicolet Nexus (FT-IR) spectrometer using KBr pellets. About 1–2 mg sample powder was mixed with about 200–300 mg of KBr to prepare the pellets and IR spectra were recorded at room temperature in the range 4000–400 cm^{-1}. The morphological and elemental analyses of the samples were performed using a field emission scanning electron microscope (FEI Quanta 200F) operating at 20 kV coupled with an energy-dispersive X-ray analysis (EDXA) unit. Transmission electron microscopic images were recorded using an FEI TECNAI G^2 electron microscope operating at an accelerating voltage of 200 kV. For the TEM analysis, the powder samples ($\sim$1–2 mg) were dispersed in about 5 mL ethanol by sonication and a drop of the dispersion was allowed to dry in air on carbon-coated copper grids. The optical properties of $Ti_xMg_{1-x}O$ samples were studied by diffuse

Table 1 Designation of $Ti_xMg_{1-x}O$ samples synthesized by thermal decomposition method and morphologies of Ti–Mg glycolates as observed by FE-SEM

| Sl. No.	Sample ID	Mg(ac)$_2$ (mmol)	Titanium isopropoxide (mmol)	Morphology (from FE-SEM)
1.	[Ti:Mg = 0.0:1.0]	1.00	0.00	Nanoflowers
2.	[Ti:Mg = 0.02:0.98]	0.98	0.02	Nanoflowers
3.	[Ti:Mg = 0.04:0.96]	0.96	0.04	Nanoflowers, rods
4.	[Ti:Mg = 0.10:0.90]	0.90	0.10	Nanoflowers, rods
5.	[Ti:Mg = 0.20:0.80]	0.80	0.20	Nanoflowers, rods
6.	[Ti:Mg = 0.33:0.66]	0.66	0.33	Rods
7.	[Ti:Mg = 0.50:0.50]	0.50	0.50	Rods
8.	[Ti:Mg = 1.0:0.0]	0.00	1.00	Rods

reflectance spectroscopy (DRS) and photoluminescence spectroscopy (PL). The diffuse reflectance spectra were recorded in the range from 200 to 800 nm using a Shimadzu UV-2450 UV–Vis spectrophotometer and $BaSO_4$ was used as the reference. About 40 mg sample powder was grounded with about 4 g $BaSO_4$ to record the diffuse reflectance spectra. A Shimadzu RF-5301 spectrofluorometer was used to obtain the PL spectra with three excitation wavelengths (250, 500, and 550 nm). About 5 mg of each powder samples were dispersed in 5 mL of water by sonication and the emission spectra were recorded at room temperature for the suspensions.

Results and discussion

The results pertinent to the Ti–Mg glycolates and the Ti^{4+}-doped MgO heteronanostructures have been discussed separately.
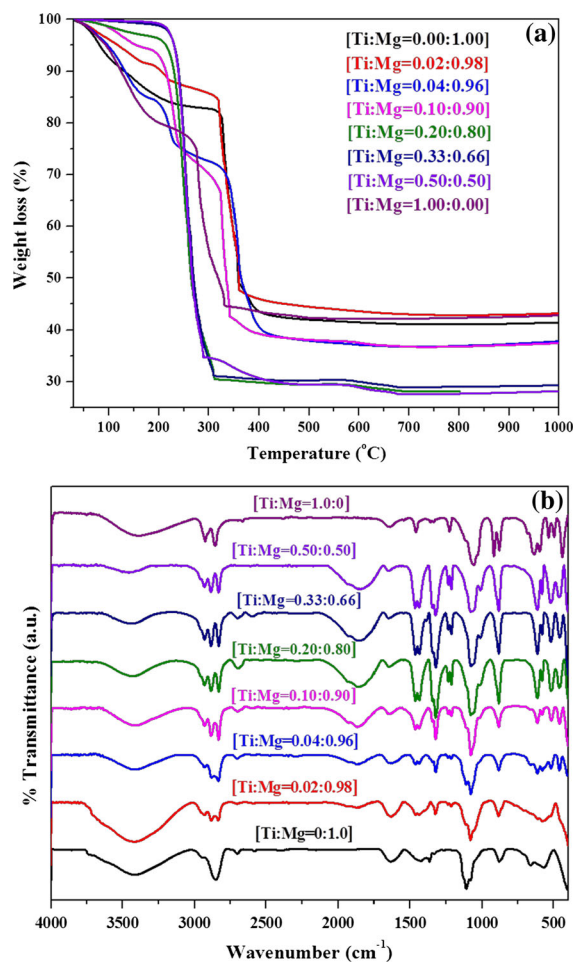
Ti–Mg glycolates

Figure 1 shows XRD patterns of the as-prepared Ti–Mg glycolates (i.e., before calcination). In the metal glycolates, the metal–ethylene glycol (EG) chains are formed by a linear growth of MO_6 octahedra. Each chain is surrounded by six other chains and the chains are held together by van der Waals interactions forming an extended array (Wang et al. 2004). In the
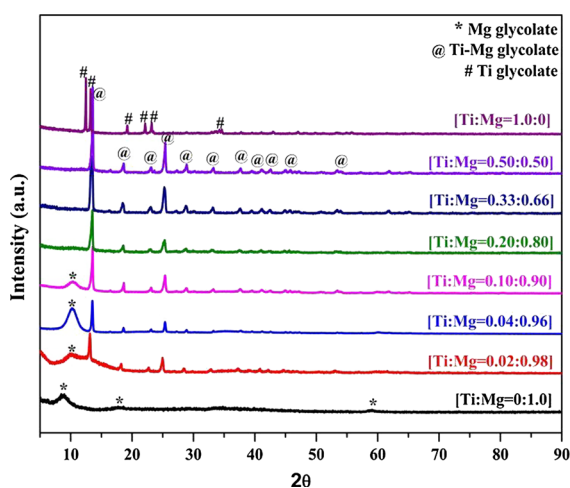
Fig. 1 XRD patterns of Ti–Mg glycolates synthesized using 0.0, 0.02, 0.04, 0.10, 0.20, 0.33, 0.50, and 1.0 mmol of titanium isopropoxide before calcination

XRD pattern of the sample synthesized by the thermal decomposition of pure magnesium acetate in EG, weak diffraction peaks due to magnesium glycolate are observed (Bain et al. 2008; Chakroune et al. 2005). Magnesium glycolate is a magnesium alkoxide in which $(C_2H_4O_2)^{2-}$ dianions chelate Mg^{2+} to form distorted $[MgO_6]$ octahedra similar to brucite-like hydroxides (Cao et al. 2006). In the XRD pattern of the sample synthesized using pure titanium isopropoxide, XRD peaks due to titanium glycolate are observed. In pure titanium glycolate, edge-sharing $[TiO_6]$ octahedra are arranged in a linear manner to form one-dimensional chain-like structure (Pol et al. 2007). The XRD pattern of Ti–Mg glycolate synthesized using 0.02 mmol of titanium isopropoxide and 0.98 mmol of magnesium acetate resembles that of pure magnesium glycolate. After the addition of 0.04–0.50 mmol of titanium isopropoxide, peaks due to titanium magnesium glycolate (Ti–Mg glycolate) are observed in the XRD patterns. The high intensity of observed XRD peaks in these patterns suggests that the Ti–Mg glycolates possess good crystallinity. In Ti–Mg glycolate, the $[TiO_6]$ octahedra are bridged together via $[Mg(OC_2H_4)_2]$ moieties and these moieties condense in a linear fashion to form Ti–Mg–EG polymer chains (Qu et al. 2012; Yadav et al. 2011). On increasing the concentration of titanium isopropoxide used during the synthesis of Ti–Mg glycolates, the intensity of the peaks due to magnesium glycolate decreases and that of the peaks due to titanium glycolate increases. In the XRD patterns of Ti–Mg glycolates prepared using 0.04 and 0.10 mmol of titanium isopropoxide, an additional broad peak is observed at low angle ($2\theta \sim 10.1°$) attributed to the presence of a small amount of magnesium glycolate. This peak is not observed in the XRD patterns of other Ti–Mg glycolate precursors (Ti:Mg = 0.20:0.80, 0.33:0.66, and 0.50:0.50). The Ti–Mg glycolates synthesized using 0.20, 0.33, and 0.50 mmol of titanium isopropoxide show similar XRD patterns which indicate that the glycolates possess the same phase irrespective of the concentration of titanium isopropoxide used during their synthesis. Similar XRD results have been reported by Qu et al. for Ti–Mg glycolates (Qu et al. 2013).

The TGA patterns for Ti–Mg glycolates are shown in Fig. 2a and the TGA results are summarized in Table 2. Pure magnesium glycolate shows a two-step weight loss. The first weight loss (18 %) in the

Fig. 2 a TGA patterns and **b** IR spectra of Ti–Mg glycolate precursors synthesized using 0.0, 0.02, 0.04, 0.10, 0.20, 0.33, 0.50, and 1.0 mmol of titanium isopropoxide

temperature range 30–320 °C is due to the desorption of physisorbed water and ethylene glycol molecules. The second weight loss (40 %) in the temperature range 320–400 °C is due to the decomposition of magnesium glycolate (Bain et al. 2008; Subramania et al. 2007). In a similar manner, a two-step weight loss pattern is observed for pure titanium glycolate. The first weight loss (23 %) at around 30–265 °C is attributed to the removal of adsorbed water and ethylene glycol, and the second weight loss (36 %) at around 265–330 °C is attributed to the decomposition of titanium glycolate (Jiang et al. 2004). TGA patterns with three to four major weight loss steps are observed in the case of Ti–Mg glycolates. The first weight loss step (1–15 %) in the temperature range 30–210 °C is due to the removal of adsorbed water and ethylene glycol. The second weight loss step (∼15–25 %) in the temperature range around 200–250 °C is attributed to the decomposition of Ti–Mg–EG polymer moieties, and the third weight loss (∼30–40 %) in the temperature range 250–350 °C is due to the formation of Ti–EG complex from the decomposition of Ti–Mg glycolate (Qu et al. 2012). The small weight loss (about 3 %) at around 350–650 °C is attributed to the formation of $MgTiO_3$ from the decomposition of titanium–EG complex. In the Ti–Mg glycolate, prepared using 0.02 mmol of titanium isopropoxide, a two-step weight loss pattern similar to that of pure magnesium glycolate is observed. For the Ti–Mg glycolates prepared using 0.04 and 0.10 mmol of titanium isopropoxide, weight loss patterns with four steps are observed. For the Ti–

Table 2 Summary of the TGA results of Ti–Mg glycolates

| Sl. No.	Sample ID	Removal of physisorbed H_2O and ethylene glycol		Decomposition of organic moieties		Overall weight loss (%)
		Temp. (°C)	% wt. loss	Temp. (°C)	% wt. loss	
1.	[Ti:Mg = 0.0:1.0]	30–320	18	320–400	40	58
2.	[Ti:Mg = 0.02:0.98]	30–200	10	200–360	43	53
3.	[Ti:Mg = 0.04:0.96]	30–190	15	190–420	47	62
4.	[Ti:Mg = 0.10:0.90]	30–190	7	190–400	54	61
5.	[Ti:Mg = 0.20:0.80]	30–200	4	210–650	68	72
6.	[Ti:Mg = 0.33:0.66]	30–210	2	210–650	70	72
7.	[Ti:Mg = 0.50:0.50]	30–210	1	210–650	69	70
8.	[Ti:Mg = 1.0:0.0]	30–265	23	265–330	36	59
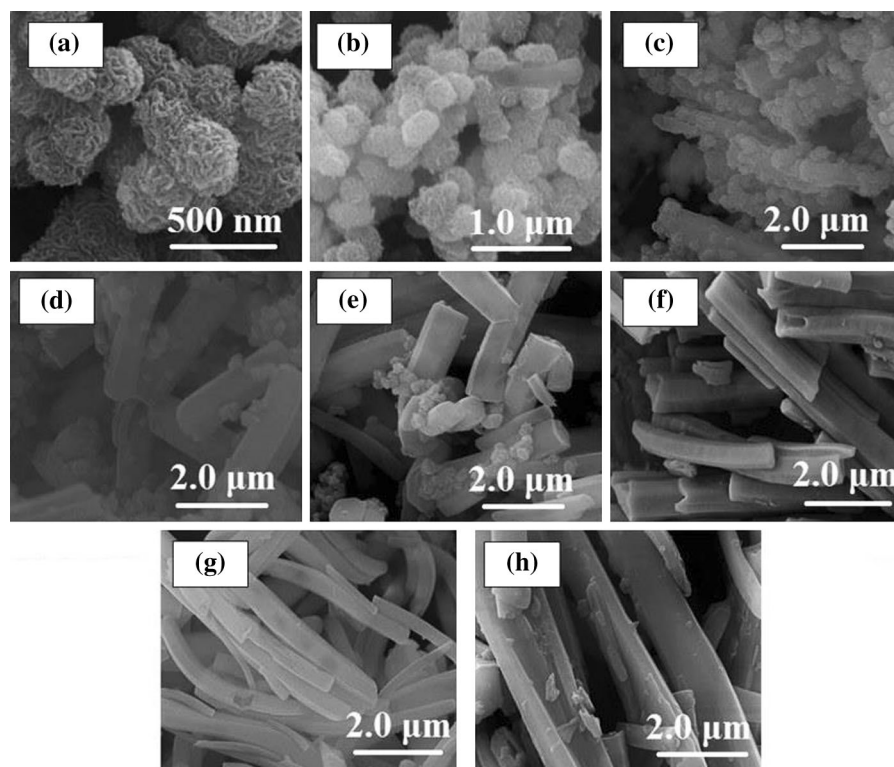
Fig. 3 FE-SEM images of Ti–Mg glycolates: **a** pure magnesium glycolate, Ti–Mg glycolates prepared using **b** 0.02, **c** 0.04, **d** 0.10, **e** 0.20, **f** 0.33, and **g** 0.50 mmol of titanium isopropoxide, and **h** pure titanium glycolate

Mg glycolates prepared using 0.20, 0.33, and 0.50 mmol of titanium isopropoxide, three-step weight loss patterns attributed to desorption of physisorbed solvent and decomposition of organic component with the formation of Ti–EG complex by the decomposition of Ti–Mg glycolate are observed. The temperature required for the complete decomposition of the Ti–Mg glycolates decreases from 400 to 300 °C, and the overall weight loss increases from about 53 to 70 % on increasing the concentration of titanium isopropoxide. In the Ti–Mg glycolates, the presence of more and more amount of glycolate units with weaker bonding between the Ti–Mg–EG moieties leads to easy removal of the organic component with increasing weight loss.

The IR spectra of Ti–Mg glycolates are shown in Fig. 2b. In the IR spectra of titanium glycolate, magnesium glycolate, and Ti–Mg glycolates, bands due to O–H stretching and bending vibrations are observed at around 3423 and 1636 cm^{-1}, respectively (Jiang et al. 2003). The IR bands at around 2916 and 2852 cm^{-1} are due to C–H stretching and the band at

about 2797 cm^{-1} is due to C–H stretching of methoxy group (Bain et al. 2008). The IR band due to asymmetric stretching of CO_3^{2-} is observed at about 1450 cm^{-1}. The IR bands at around 1090 and 1020 cm^{-1} are attributed to C–C and C–O vibrations of organic moieties and the bands at around 1234 and 1220 cm^{-1} are attributed to C–O–Ti bond (Bain et al. 2008). The IR band observed at around 660 cm^{-1} is attributed to Ti–O bond and the bands at around 574, 521, and 467 cm^{-1} are attributed to Mg–O and Ti–O–Ti bonds (Li et al. 2010).

Figure 3 shows the FE-SEM images of Ti–Mg glycolates and Tables 4 and 5 show the summary of EDX analysis results. Uniform flowers with a diameter of 250 ± 50 nm, formed by the aggregation of flakes, are observed in pure magnesium glycolate which is in agreement with the literature (Bain et al. 2008). In pure titanium glycolate, rods with length 3.1 ± 0.5 µm and width 220 ± 60 nm are observed. In the samples prepared using 0.02, 0.04, 0.10, and 0.20 mmol of titanium isopropoxide, particles with a mixture of rod-like and flower-like morphologies are
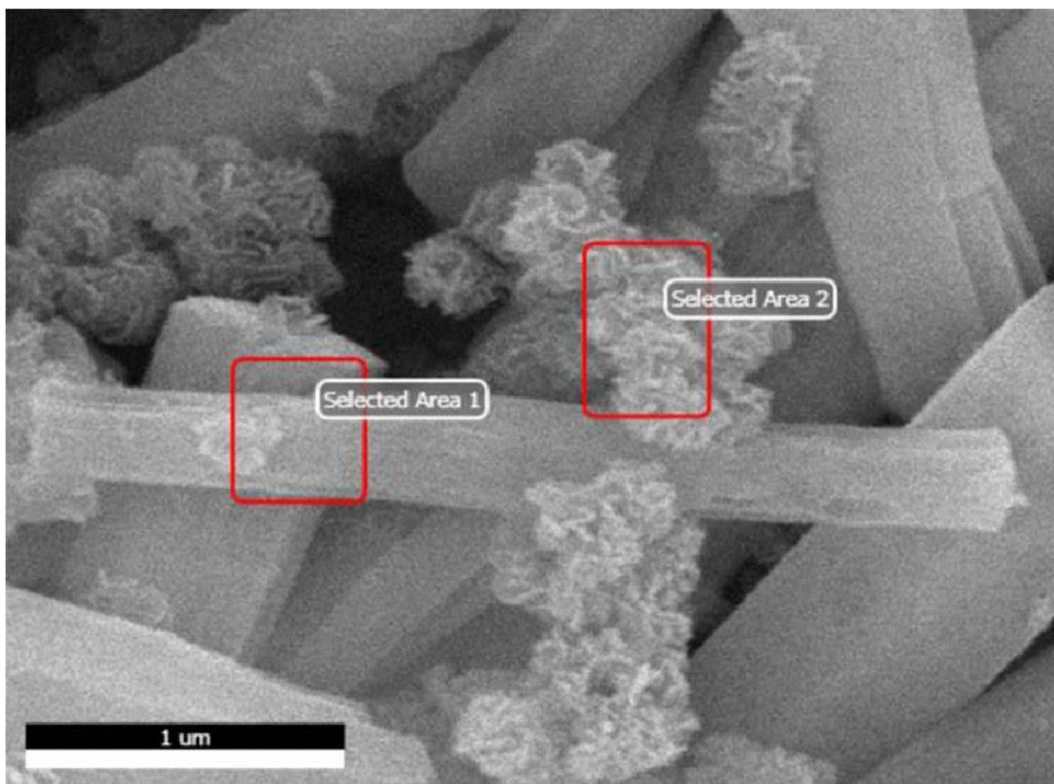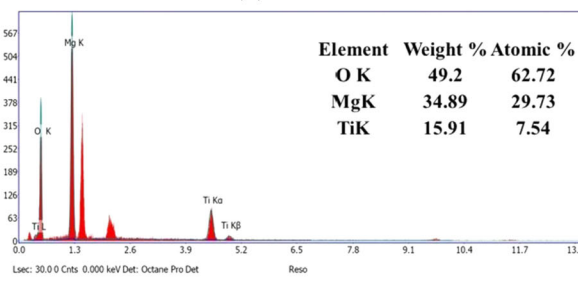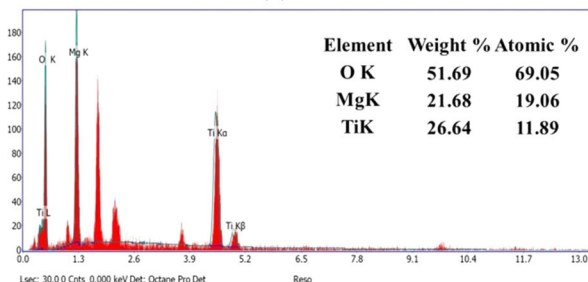
Fig. 4 FE-SEM image of Ti–Mg glycolate [Ti:Mg = 0.20:0.80] and the corresponding EDXA plots at two different areas: **a** rods and **b** flowers

formed. On increasing the concentration of titanium isopropoxide, the number of rods increases and that of flowers decreases. Hexagonal rods with length 4.2 ± 0.7 μm and width 380 ± 75 nm are formed at higher concentrations of titanium isopropoxide (0.33 to 0.50 mmol). Qu et al. have reported the synthesis of Ti–Mg glycolate nanorods with Ti:Mg = 2:1, 1:1, and 1:2 (Qu et al. 2013). In the Ti–Mg glycolates prepared using 0.33 and 0.50 mmol of titanium isopropoxide, only hexagonal rods are observed. On increasing the concentration of titanium isopropoxide from 0.33 to

0.50 mmol, the length of rods increases from 4.2 ± 0.7 to 5.3 ± 1.2 μm and the width increases from 380 ± 75 to 480 ± 100 nm.

The Ti–Mg glycolates, prepared using 0.02, 0.33, and 0.50 mmol of titanium isopropoxide, show uniform elemental composition (Tables 4, 5). The elemental compositions of Ti–Mg glycolates prepared using 0.04, 0.10, and 0.20 mmol of titanium isopropoxide indicate that they are nonuniform. It was found from EDX analysis that the rods are titanium rich and the flowers are magnesium rich (Fig. 4). This

is because of the presence of magnesium glycolate in the flowers and Ti–Mg glycolate in the rods. The presence of both magnesium glycolate and Ti–Mg glycolate is noticed in the XRD patterns of precursors prepared using 0.04 and 0.10 mmol of titanium isopropoxide, but for the precursor prepared using 0.20 mmol of titanium isopropoxide, the presence of magnesium glycolate was not detected in the XRD pattern.

Ti^{4+}-doped MgO heteronanostructures

The XRD patterns of $Ti_xMg_{1-x}O$ samples, obtained after calcination of the corresponding Ti–Mg glycolates at 500 °C, are shown in Fig. 5a and an overall summary of the XRD results is provided in Table 3. Pure magnesium glycolate forms MgO (JCPDS file no. 74-1225) after calcination at 500 °C. The crystallite size of pure MgO, as calculated using the Debye–Scherrer equation, is 12.3 nm. In the sample synthesized using only pure titanium isopropoxide and calcined at 500 °C, XRD peaks due to anatase TiO_2 (JCPDS file no. 86-1157) are observed. The $Ti_xMg_{1-x}O$ samples prepared using 0.02, 0.04, and 0.10 mmol of titanium isopropoxide show XRD peaks due to pure MgO, but at higher concentrations of titanium isopropoxide (0.20–0.50 mmol), amorphous nature of the samples is observed. During the addition of titanium isopropoxide (0.02–0.10 mmol), the crystallite size of MgO decreases from 12.3 nm to 5.3 nm. The presence of titanium inhibits the crystallization of $Ti_xMg_{1-x}O$ (Wang et al. 2009), and hence the intensity of XRD peaks as well as the crystallite size of $Ti_xMg_{1-x}O$ decreases on increasing the concentration of titanium isopropoxide. The inhibition of crystallization of $Ti_xMg_{1-x}O$ samples is due to difference in ionic radius of Mg^{2+} (0.72 Å) and Ti^{4+} (0.64 Å) (Wang et al. 2009; Yang and Shen 2005), and the crystallinity of the samples decreases on increasing the concentration of titanium isopropoxide used during the synthesis. In the sample [Ti:Mg = 0.10:0.90] calcined at 500 °C, the presence of titanium has been proved from the EDX results (Tables 4, 5). DRS results (Fig. 11) also show an absorption band at around 330 nm due to the presence of $MgTiO_3$. However, only MgO phase is detected in the XRD pattern due to the inhibition of crystallization of $MgTiO_3$ at 500 °C due to the presence of titanium.
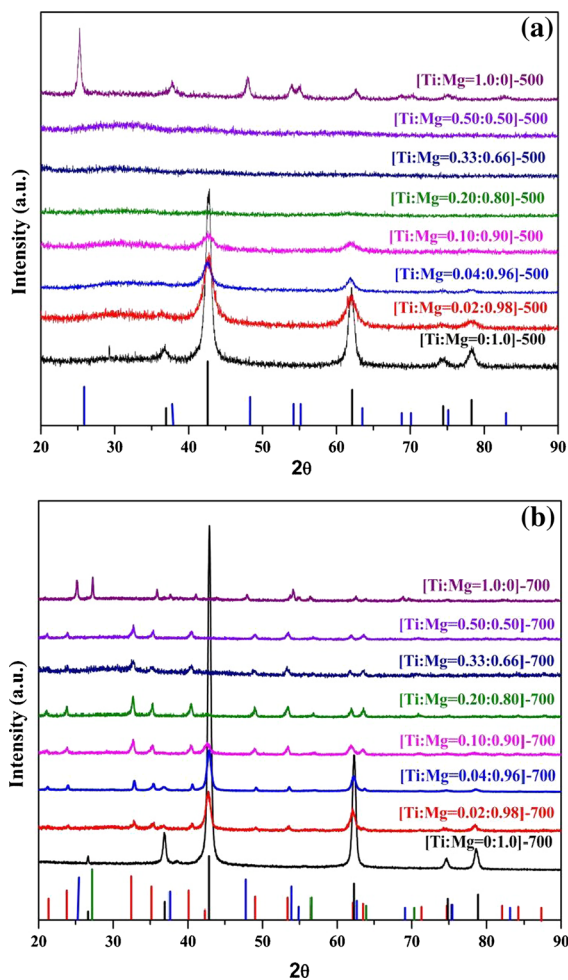
Fig. 5 XRD patterns of **a** $Ti_xMg_{1-x}O$ samples prepared using 0.0, 0.02, 0.04, 0.10, 0.20, 0.33, 0.50, and 1.0 mmol of titanium isopropoxide and calcined at 500 °C (*black line* is for MgO from the JCPDS database and *blue line* is for anatase TiO_2) and **b** $Ti_xMg_{1-x}O$ samples calcined at 700 °C (*black line* is for MgO from the JCPDS database, *red line* is for $MgTiO_3$, *blue line* is for anatase TiO_2, and *green line* is for rutile TiO_2)

The XRD patterns of $Ti_xMg_{1-x}O$ samples calcined at 700 °C are shown in Fig. 5b. After calcination at 700 °C, pure magnesium glycolate forms MgO with a crystallite size of 11.0 nm. After calcination of pure titanium glycolate at 700 °C, XRD peaks due to anatase TiO_2 along with peaks due to rutile (JCPDS file no. 89-4920) are observed. The $Ti_xMg_{1-x}O$ samples synthesized using 0.02, 0.04, and 0.10 mmol of titanium isopropoxide and calcined at 700 °C form a mixture of $MgTiO_3$ (JCPDS file no. 79-0831) and MgO. The percentage of $MgTiO_3$ was calculated from

Table 3 Summary of the XRD results and the DRS results for the $Ti_xMg_{1-x}O$ samples obtained by the calcination of Ti–Mg glycolates at 500 and 700 °C

Sl. no.	Sample ID	500 °C			700 °C		
		Phase	Crystallite size (nm)	Band gap (eV)	Phase	Crystallite size (nm)	Band gap (eV)
1.	[Ti:Mg = 0.0:1.0]	MgO	12.3	–	MgO	11.0	–
2.	[Ti:Mg = 0.02:0.98]	MgO	5.8	4.0	MgO (82 %), MgTiO₃ (18 %)	11.4, 22.8	4.2
3.	[Ti:Mg = 0.04:0.96]	MgO	6.1	3.7	MgO (80 %), MgTiO₃ (20 %)	13.4, 27.4	4.0
4.	[Ti:Mg = 0.10:0.90]	MgO	5.3	3.6	MgO (45 %), MgTiO₃ (55 %)	9.5, 28.5	4.1
5.	[Ti:Mg = 0.20:0.80]	Amorphous	–	3.6	MgTiO₃	29.1	3.7
6.	[Ti:Mg = 0.33:0.66]	Amorphous	–	3.6	MgTiO₃	25.0	3.6
7.	[Ti:Mg = 0.50:0.50]	Amorphous	–	3.2	MgTiO₃	29.8	3.6
8.	[Ti:Mg = 1.0:0.0]	Anatase TiO₂	15.0	3.0	Anatase TiO₂ (45 %), rutile TiO₂ (55 %)	36.0, 45.7	3.3

Table 4 EDXA results and overall elemental composition of Ti–Mg glycolates and $Ti_xMg_{1-x}O$ samples calcined at 500 and 700 °C

Sl. no.	Sample ID	Theoretical Ti/Mg molar ratio	[Ti:Mg] molar ratio in Ti–Mg glycolates	[Ti:Mg] molar ratio in samples calcined at 500 °C	[Ti:Mg] molar ratio in samples calcined at 700 °C	Elemental distribution
1.	[Ti:Mg = 0.0:1.0]	–	–	–	–	–
2.	[Ti:Mg = 0.02:0.98]	0.02:1	0.02:1	0.02:1	0.02:1	Uniform
3.	[Ti:Mg = 0.04:0.96]	0.04:1	0.10:1	0.09:1	0.11:1	Nonuniform
4.	[Ti:Mg = 0.10:0.90]	0.11:1	0.14:1	0.15:1	0.13:1	Nonuniform
5.	[Ti:Mg = 0.20:0.80]	0.25:1	0.32:1	0.29:1	0.33:1	Nonuniform
6.	[Ti:Mg = 0.33:0.66]	0.50:1	0.80:1	0.90:1	0.80:1	Uniform
7.	[Ti:Mg = 0.50:0.50]	1:1	0.90:1	1:1	1.1:1	Uniform
8.	[Ti:Mg = 1.0:0.0]	–	–	–	–	–

The analysis was carried out on large areas of samples

the most intense XRD peak [(104) reflection] for MgTiO₃ (JCPDS file no. 79-0831). The sum of the intensities of most intense reflections due to MgO ($I_{(200)}$) and MgTiO₃ ($I_{(104)}$) was assumed to be 100. From the ratio of $I_{(104)}/I_{(total)}$, the percentage of MgTiO₃ was estimated and $I_{(total)}$ refers to the sum of $I_{(MgO)}$ and $I_{(MgTiO3)}$. The percentage of MgTiO₃ increases from 18 to 55 % and that of MgO decreases from 82 to 45 % on increasing the concentration of titanium isopropoxide used during the synthesis of Ti–Mg glycolates. The $Ti_xMg_{1-x}O$ samples prepared using 0.20, 0.33, and 0.50 mmol of titanium isopropoxide form pure MgTiO₃. As discussed above, the presence of titanium during the synthesis inhibits the crystallization of $Ti_xMg_{1-x}O$ samples. At 500 °C, the energy required for the crystallization of $Ti_xMg_{1-x}O$

sample is not sufficient, and hence only the XRD pattern of MgO is observed for the samples prepared using lower concentration of titanium isopropoxide (0.02–0.10 mmol) and amorphous pattern is observed in the XRD patterns for samples prepared using higher concentrations of titanium isopropoxide (0.20–0.50 mmol). At a higher calcination temperature (700 °C), crystallization of $Ti_xMg_{1-x}O$ takes place and the mixture of MgO and MgTiO₃ is observed for the $Ti_xMg_{1-x}O$ samples prepared using 0.02–0.10 mmol of titanium isopropoxide and MgTiO₃ is formed in the samples prepared using 0.20–0.50 mmol of titanium isopropoxide.

The FE-SEM images of $Ti_xMg_{1-x}O$ samples calcined at 500 °C are shown in Fig. 6, and an overall summary of EDX analysis results on large areas of

Table 5 EDXA results for Ti–Mg glycolate precursors and $Ti_xMg_{1-x}O$ samples calcined at 500 and 700 °C

Sl. no.	Sample ID	Theoretical Ti/Mg molar ratio	[Ti:Mg] molar ratio in Ti–Mg glycolates		[Ti:Mg] molar ratio in samples calcined at 500 °C		[Ti:Mg] molar ratio in samples calcined at 700 °C		Elemental distribution
			Flowers	Rods	Flowers	Rods	Flowers	Rods	
1.	[Ti:Mg = 0.0:1.0]	–	–	–	–	–	–	–	–
2.	[Ti:Mg = 0.02:0.98]	0.02:1	0.02:1	–	0.02:1	–	0.02:1	–	Uniform
3.	[Ti:Mg = 0.04:0.96]	0.04:1	0.02:1	0.16:1	0.03:1	0.14:1	0.02:1	0.15:1	Nonuniform
4.	[Ti:Mg = 0.10:0.90]	0.11:1	0.09:1	0.14:1	0.09:1	0.30:1	0.11:1	0.22:1	Nonuniform
5.	[Ti:Mg = 0.20:0.80]	0.25:1	0.22:1	0.40:1	0.16:1	0.50:1	0.19:1	0.50:1	Nonuniform
6.	[Ti:Mg = 0.33:0.66]	0.50:1	–	0.80:1	–	0.90:1	–	0.80:1	Uniform
7.	[Ti:Mg = 0.50:0.50]	1:1	–	0.90:1	–	1:1	–	1.1:1	Uniform
8.	[Ti:Mg = 1.0:0.0]	–	–	–	–	–	–	–	–

The analysis was carried out on different selected areas of samples
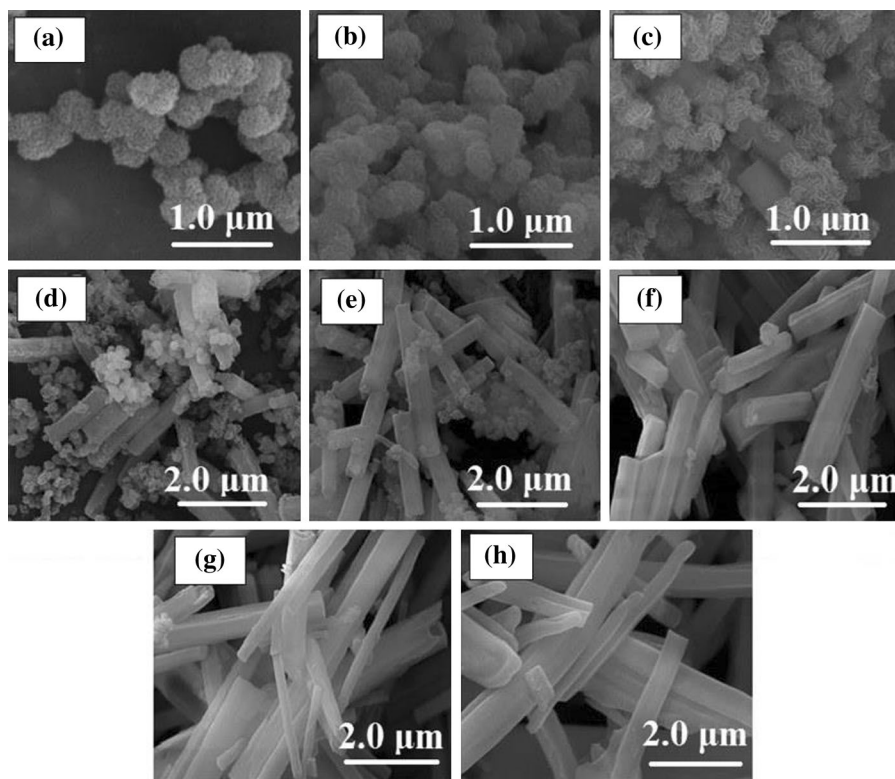
Fig. 6 FE-SEM images of $Ti_xMg_{1-x}O$ samples after calcination at 500 °C: **a** pure MgO, $Ti_xMg_{1-x}O$ samples prepared using **b** 0.02, **c** 0.04, **d** 0.10, **e** 0.20, **f** 0.33, and **g** 0.50 mmol of titanium isopropoxide, and **h** pure TiO_2

samples and on different selected areas of samples is provided in Tables 4 and 5, respectively. Particles with flower-like morphology (diameter around 250 ± 50 nm) consisting of small nanoparticles are observed in pure MgO calcined at 500 °C. In the $Ti_xMg_{1-x}O$ samples, synthesized using 0.02–0.20 mmol of titanium isopropoxide and calcined at 500 °C, particles with hexagonal rod-like morphology
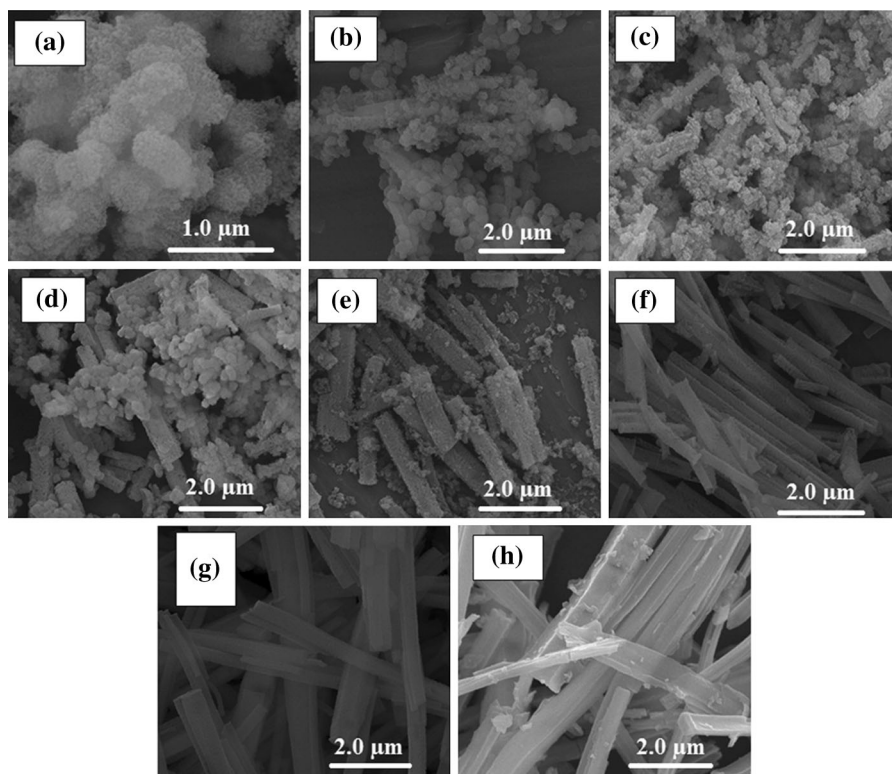
Fig. 7 FE-SEM images of $Ti_xMg_{1-x}O$ samples after calcination at 700 °C: **a** pure MgO, $Ti_xMg_{1-x}O$ samples prepared using **b** 0.02, **c** 0.04, **d** 0.10, **e** 0.20, **f** 0.33, and **g** 0.50 mmol of titanium isopropoxide, and **h** pure TiO_2

with length 4.2 ± 0.7 μm and width 380 ± 75 nm along with flowers are observed. In the $Ti_xMg_{1-x}O$ samples, synthesized using 0.33 and 0.50 mmol of titanium isopropoxide and pure titanium isopropoxide, particles with rod-like morphology are observed. The length of the rods is 4.2 ± 0.7, 5.3 ± 1.2, and 3.1 ± 0.5 μm and the width is 380 ± 75, 480 ± 100, and 220 ± 60 nm, respectively. The EDX analysis results (Tables 4 and 5) indicate that the $Ti_xMg_{1-x}O$ samples prepared using 0.02, 0.33, and 0.50 mmol of titanium isopropoxide exhibit uniform elemental distribution, whereas the $Ti_xMg_{1-x}O$ samples prepared using 0.04, 0.10, and 0.20 mmol of titanium isopropoxide show nonuniform elemental distribution (Table 4). The flowers were found to be magnesium rich, whereas the rods were titanium rich. The FE-SEM images of $Ti_xMg_{1-x}O$ samples calcined at 700 °C are shown in Fig. 7. The samples calcined at 700 °C show particles with similar dimensions as those of the samples calcined at 500 °C, but the small nanoparticles are more clearly visible in the

$Ti_xMg_{1-x}O$ samples calcined at 700 °C as compared to the samples calcined at 500 °C. This is due to better crystallization and growth at higher calcination temperature. In the $Ti_xMg_{1-x}O$ samples calcined at 500 °C, the surface of the rods is smooth, whereas in the samples calcined at 700 °C, the nanoparticles are clearly visible on the surface. The morphology of the Ti–Mg glycolate precursors is maintained in the $Ti_xMg_{1-x}O$ samples after calcination at 500 and 700 °C.

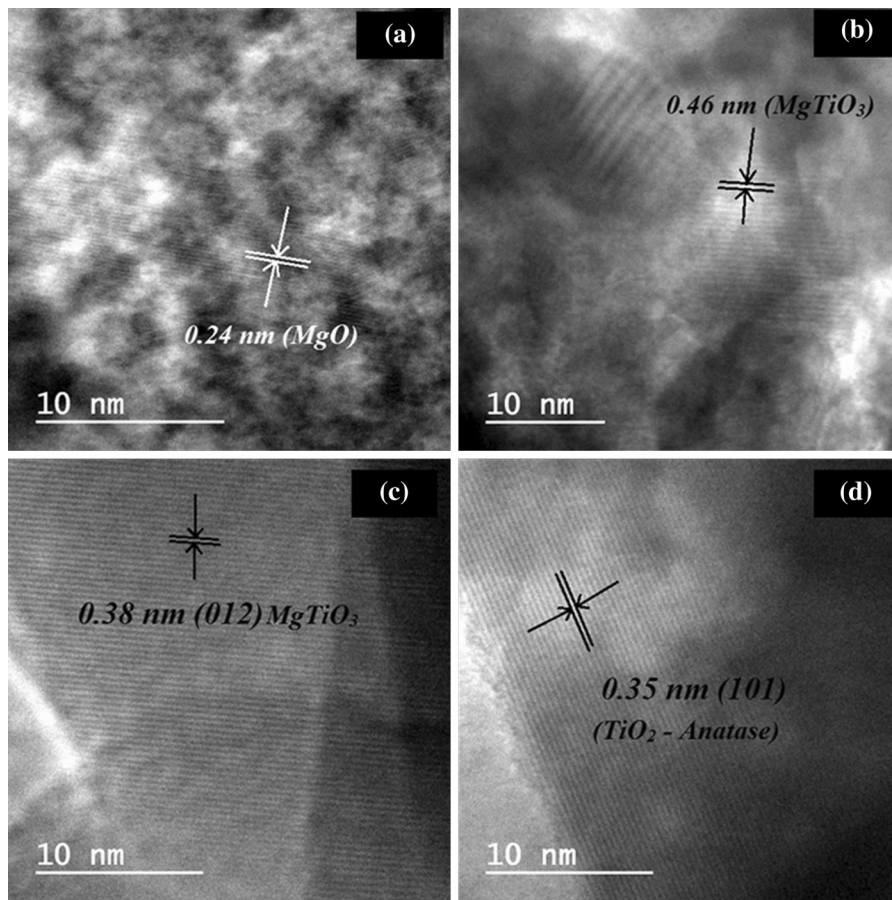The TEM images of pure MgO calcined at 700 °C, pure TiO_2 calcined at 700 °C, $Ti_xMg_{1-x}O$ [Ti:Mg = 0.04:0.96] calcined at 500 and 700 °C, and $Ti_xMg_{1-x}O$ [Ti:Mg = 0.33:0.66] calcined at 500 and 700 °C are shown in Fig. 8. The HRTEM images of pure TiO_2 calcined at 700 °C, $Ti_xMg_{1-x}O$ [Ti:Mg = 0.04:0.96] calcined at 500 and 700 °C, and $Ti_xMg_{1-x}O$ [Ti:Mg = 0.33:0.66] calcined at 700 °C are shown in Fig. 9. Selected area electron diffraction (SAED) patterns of pure MgO calcined at 700 °C, pure TiO_2 calcined at 700 °C, $Ti_xMg_{1-x}O$ [Ti:Mg = 0.04:0.96]
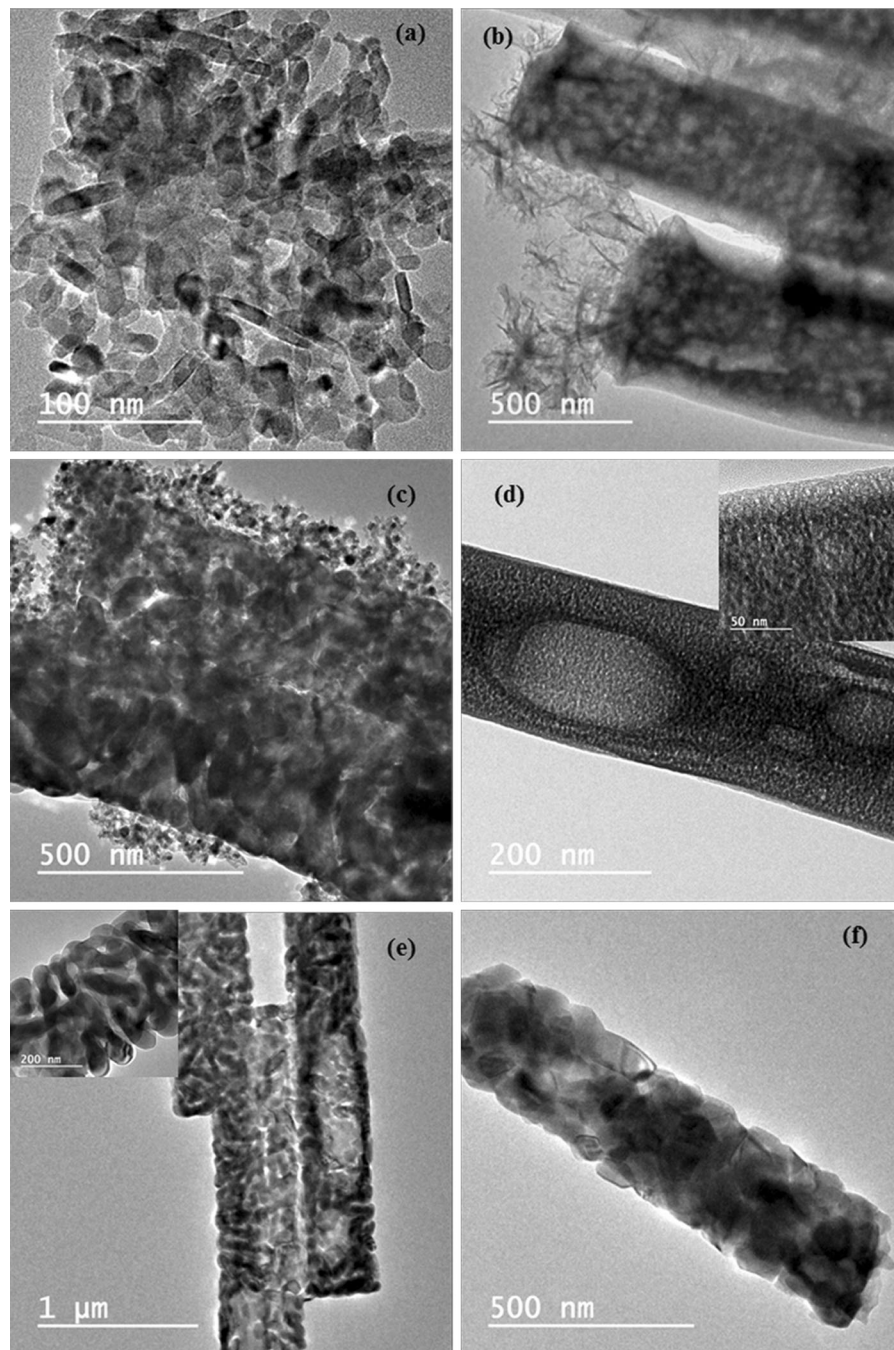
Fig. 8 TEM images of **a** pure MgO-700 °C, **b** [Ti:Mg = 0.04:0.96]-500, **c** [Ti:Mg = 0.04:0.96]-700, **d** [Ti:Mg = 0.33:0.66]-500, **e** [Ti:Mg = 0.33:0.66]-700, and **f** pure TiO$_2$-700 °C

calcined at 500 and 700 °C, and $Ti_xMg_{1-x}O$ [Ti:Mg = 0.33:0.66] calcined at 700 °C are shown in Fig. 10. In the TEM image of pure MgO calcined at 700 °C, agglomerated nanoparticles with irregular shape

and size 20.4 ± 6.4 nm and nanorods with length 36.5 ± 7.4 nm and width 10.4 ± 3.5 nm are observed. In pure TiO$_2$ calcined at 700 °C, hollow rods with length 3.1 ± 0.5 μm and width 220 ± 60 nm formed by the

Fig. 9 HRTEM images of **a** [Ti:Mg = 0.04:0.96]-500, **b** [Ti:Mg = 0.04:0.96]-700, **c** [Ti:Mg = 0.33:0.66]-700, and **d** pure TiO_2 calcined at 700 °C

assembly of particles with irregular shape are observed. In the TEM image of $Ti_xMg_{1-x}O$ [Ti:Mg = 0.04:0.96] calcined at 500 °C, flakes along with rods (length 3.5 ± 0.7 μm and width 320 ± 50 nm) formed by the assembly of nanoparticles (size 5.5 ± 1.6 nm) are observed. In the TEM image of $Ti_xMg_{1-x}O$ [Ti:Mg = 0.04:0.96] calcined at 700 °C, small nanoparticles (17.7 ± 2.5 nm) are observed with rods (length 3.7 ± 1.0 μm and width 420 ± 70 nm) and the rods consist of nanoparticles (size = 86.5 ± 9.6 nm). In the TEM image of $Ti_xMg_{1-x}O$ [Ti:Mg = 0.33:0.66] calcined at 500 °C, hollow rods with length 4.5 ± 1.0 μm and width 480 ± 100 nm are observed and these rods are formed by the assembly of small nanoparticles (size 5.2 ± 0.7 nm). In the same sample calcined at 700 °C, dumbbell-shaped nanoparticles (length 137.6 ± 12.3 nm and width 45.3 ± 5.3 nm) assemble to form hollow rods (length 4.2 ± 0.8 μm and width 380 ± 75 nm).

HRTEM image of $Ti_xMg_{1-x}O$ [Ti:Mg = 0.04:0.96]-500 (Fig. 9a) shows lattice fringes with d-spacing 0.24 nm, which corresponds to (220) reflection of MgO, and in the same sample after calcination at 700 °C (Fig. 9b), lattice fringes with d-spacing 0.46 nm are observed, which are attributed to (110) reflection in $MgTiO_3$. In the $Ti_xMg_{1-x}O$ sample [Ti:Mg = 0.33:0.66]-700 (Fig. 9c), the observed lattice fringes with d-spacing 0.38 nm are attributed to (012) reflection in $MgTiO_3$. In pure TiO_2 calcined at 700 °C (Fig. 9d), the observed lattice fringes with *d*-spacing 0.35 nm are attributed to (101) reflection in anatase TiO_2.

In the SAED pattern of pure MgO calcined at 700 °C (Fig. 10a), rings and spots are observed which are indexed to (111), (200), and (220) planes of MgO. In the SAED pattern of pure TiO_2 calcined at 700 °C (Fig. 10f), the observed spots are attributed to (101), (200), and (211) planes of anatase TiO_2 and (111),
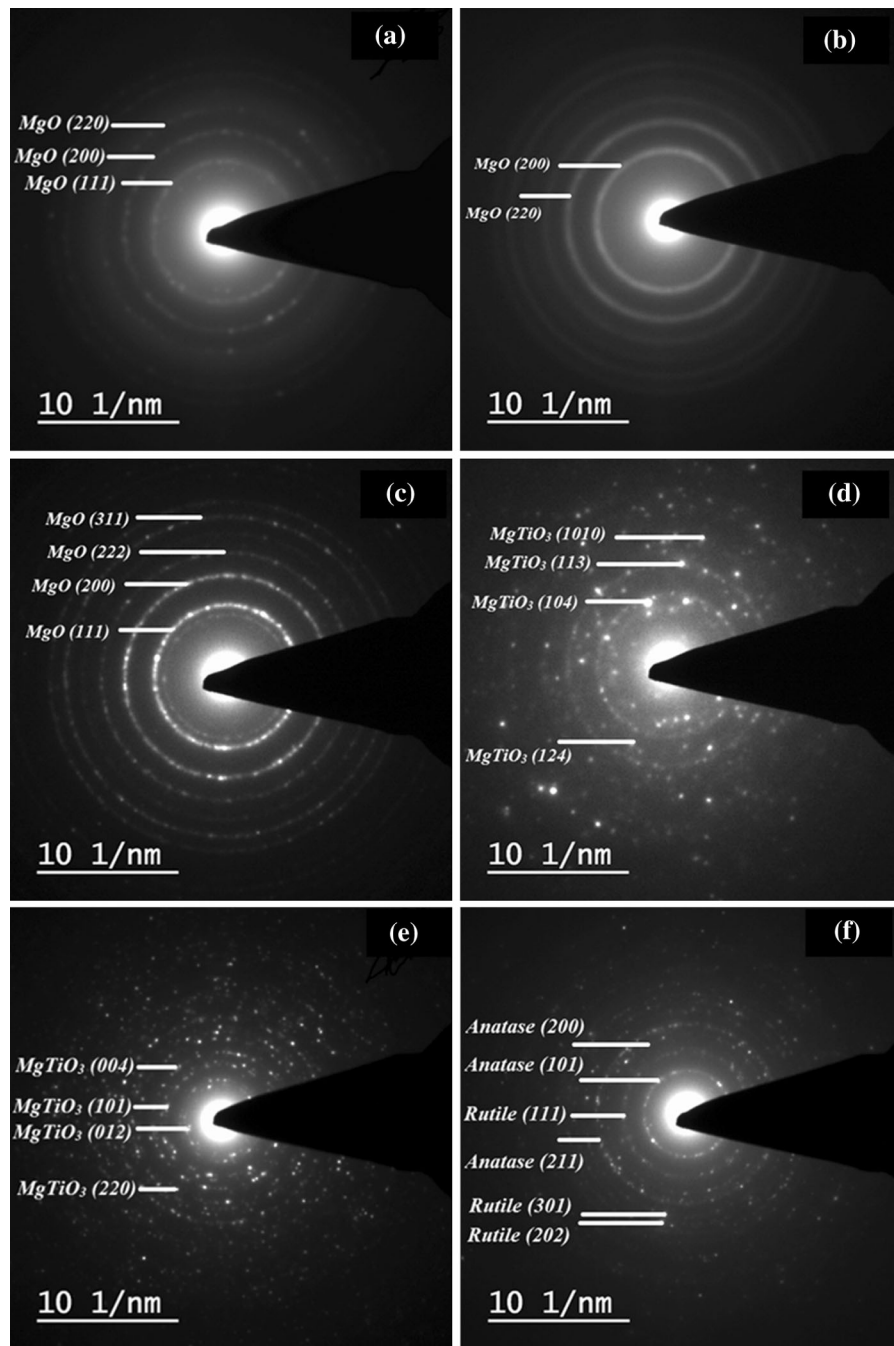
Fig. 10 SAED patterns of **a** pure MgO calcined at 700 °C, **b** [Ti:Mg = 0.04:0.96]-500, **c**, **d** [Ti:Mg = 0.04:0.96]-700, **e** [Ti:Mg = 0.33:0.66]-700, and **f** pure TiO$_2$ calcined at 700 °C

(301), and (202) planes of rutile TiO$_2$. In the SAED pattern of Ti$_x$Mg$_{1-x}$O [Ti:Mg = 0.04:0.96] calcined at 500 °C (Fig. 10b), rings due to (200) and (220) planes of MgO are observed, whereas in the same
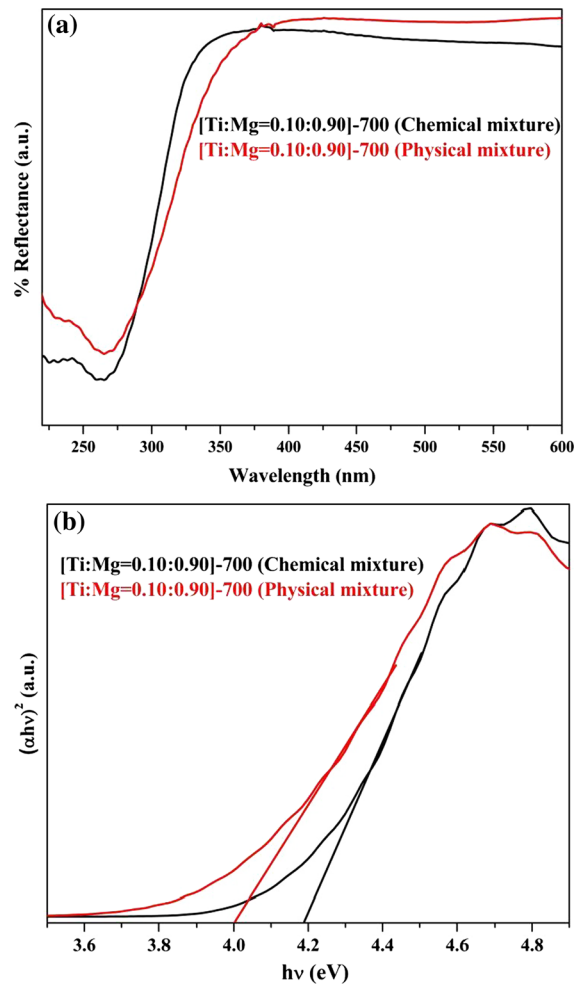
sample calcined at 700 °C, two distinct SAED patterns due to MgO and MgTiO$_3$ are observed (Fig. 10c, d). In the Ti$_x$Mg$_{1-x}$O [Ti:Mg = 0.33:0.66] calcined at 500 °C, diffused SAED pattern was observed which
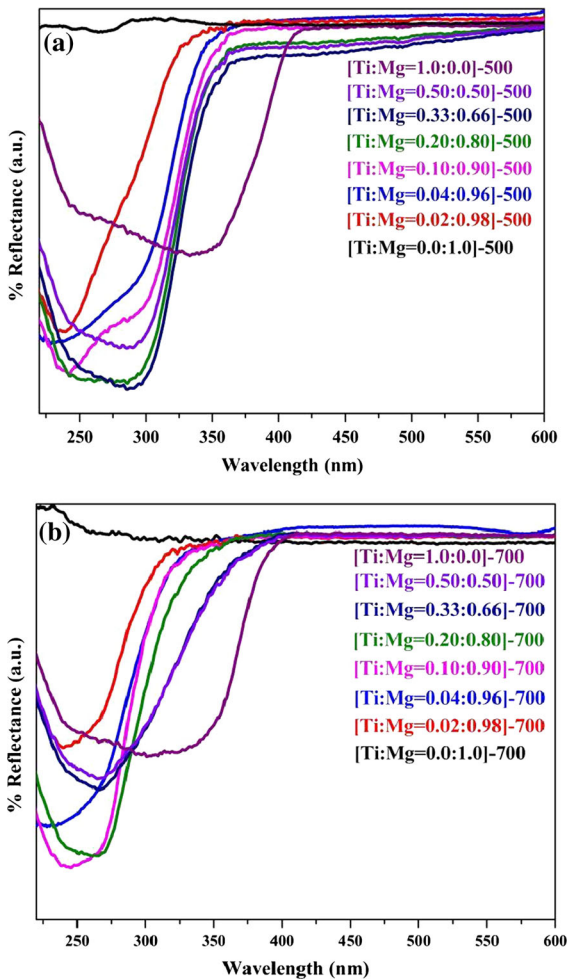
Fig. 11 DRS plots of pure MgO and Ti$_x$Mg$_{1-x}$O samples prepared using 0.02, 0.04, 0.10, 0.20, 0.33, 0.50, and 1.0 mmol of titanium isopropoxide and calcined at **a** 500 °C and **b** 700 °C

Fig. 12 a DRS spectra of a physical mixture of MgTiO$_3$ and MgO calcined at 700 °C along with that of a sample synthesized with same elemental composition ([Ti:Mg = 0.10:0.90]) and calcined at 700 °C and (b) the corresponding Tauc plots

suggests that this sample is amorphous, whereas in the same sample calcined at 700 °C, spots due to MgTiO$_3$ are observed (Fig. 10e) which proves single-crystalline nature of the rods.

Diffuse reflectance spectra of Ti$_x$Mg$_{1-x}$O samples calcined at 500 and 700 °C are shown in Fig. 11a, b, respectively, and a summary of the DRS results is provided in Table 3. Pure MgO is optically transparent in the 200–800 nm range, whereas Ti$_x$Mg$_{1-x}$O samples show absorption between 300 and 400 nm. The calculation of band gap for pure MgO was not possible because MgO does not absorb in the measured wavelength range. The reported band gap for pure MgO is 7.8 eV [Devaraja et al. 2014]. The band gap of
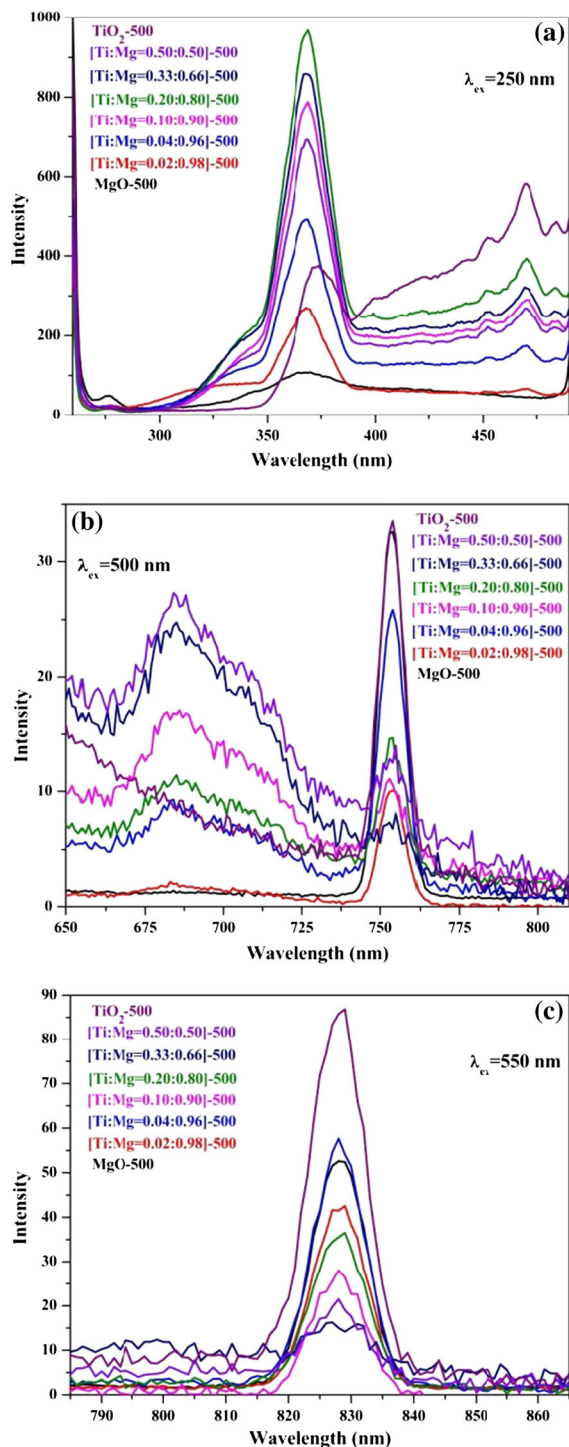
Ti$_x$Mg$_{1-x}$O samples calcined at 500 °C decreases from 4.0 to 3.2 eV on increasing the concentration of titanium isopropoxide used during the synthesis. For the samples calcined at 700 °C, a decrease in the band gap from 4.2 to 3.6 eV is observed on increasing the concentration of titanium isopropoxide. The decrease in the band gap on increasing the concentration of titanium is attributed to an increase in the crystallite size of MgTiO$_3$ (Table 3). At higher concentration, Mg^{2+} suppresses the growth of MgTiO$_3$ crystals with the formation of smaller crystallites of MgTiO$_3$, whereas higher Ti^{4+} content facilitates the formation of MgTiO$_3$ and the band gap is red shifted (Bayal and Jeevanandam 2014). The optical properties of a

control sample which is a physical mixture of pure MgO and MgTiO$_3$ (both calcined at 700 °C) corresponding to a composition Ti:Mg = 0.10:0.90 were also measured. The observed spectrum was compared with a Ti$_x$Mg$_{1-x}$O sample synthesized using Ti:Mg = 0.10:0.90 followed by calcination at 700 °C (i.e., chemical mixture). The DRS spectra of these samples and the corresponding Tauc plots are shown in Fig. 12. The observed band gap for the chemical mixture (4.2 eV) is greater than that of the physical mixture (4.0 eV). This is attributed to the synergic effect of both the phases (MgO and MgTiO$_3$) present in the chemical mixture.

In the present study, an increase in band gap for Ti$_x$Mg$_{1-x}$O samples is observed on increasing the calcination temperature from 500 to 700 °C. On calcining the Ti$_x$Mg$_{1-x}$O samples at 500 °C, structural disorder is generated due to the formation of oxygen-deficient [TiO$_5$] clusters which cause an intrinsic distortion in the metal–oxygen bonds which give rise to intermediate energy levels within the band gap. On increasing the calcination temperature to 700 °C, [TiO$_6$] clusters are formed, the number of [TiO$_5$] clusters is reduced, and the structural organization is now better in short as well as long range (Ferri et al. 2009). The increase in the band gap is attributed to depletion of the intermediate energy levels within the optical band gap of MgTiO$_3$. Ferri et al. have reported an increase in the band gap (3.07–4.05 eV) of magnesium titanate due to reduction of intermediate energy levels on increasing the annealing temperature from 450 to 700 °C (Ferri et al. 2009).

The luminescence properties of Ti$_x$Mg$_{1-x}$O samples were studied at three excitation wavelengths, 250, 500, and 550 nm (Devaraja et al. 2014; Ho and Huang 2013). The PL spectra of Ti$_x$Mg$_{1-x}$O samples calcined at 500 and 700 °C with the excitation wavelengths of 250, 500, and 550 nm are shown in Figs. 13 and 14, respectively, and an overall summary of the PL results is provided in Table 6. Figures 13a and 14a show the PL spectra of Ti$_x$Mg$_{1-x}$O samples calcined at 500 and 700 °C, respectively, with an excitation wavelength of 250 nm. Emission bands at about 367 and 470 nm are observed in pure MgO and in the Ti$_x$Mg$_{1-x}$O samples, calcined at 500 and 700 °C. The emission band at about 367 nm is attributed to surface oxygen vacancies occupied by single electrons, while the emission band at about 470 nm is due to unoccupied oxygen

Fig. 13 PL spectra of Ti$_x$Mg$_{1-x}$O samples synthesized using 0.0, 0.02, 0.04, 0.10, 0.20, 0.33, 0.50, and 1.0 mmol of titanium isopropoxide and calcined at 500 °C with different excitation wavelengths: **a** 250 nm, **b** 500 nm, and **c** 550 nm
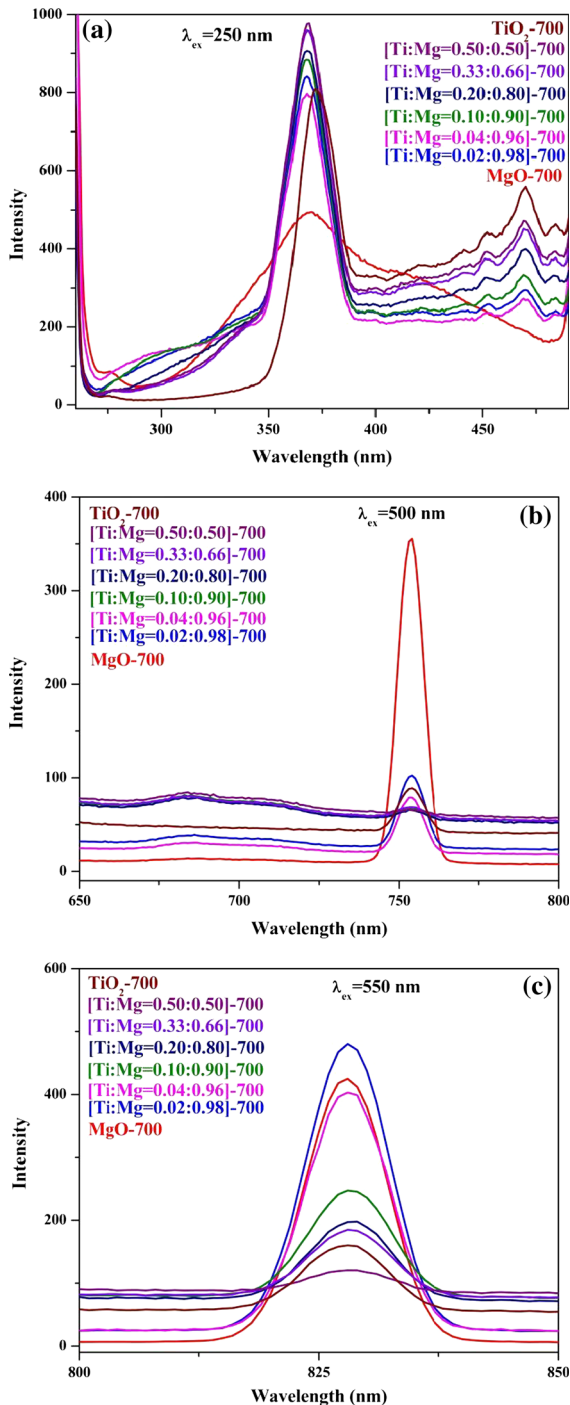
Fig. 14 PL spectra of $Ti_xMg_{1-x}O$ samples synthesized using 0.0, 0.02, 0.04, 0.10, 0.20, 0.33, 0.50, and 1.0 mmol of titanium isopropoxide and calcined at 700 °C with different excitation wavelengths: **a** 250 nm, **b** 500 nm, and **c** 550 nm

vacancies on the surface (Devaraja et al. 2014). Band edge emission for $Ti_xMg_{1-x}O$ samples is not observed because the emission bands associated with surface defects dominate the PL spectra. The intensity of emission at 367 nm increases on increasing the concentration of titanium isopropoxide which indicates that the number of oxygen vacancies increases with an increase in the concentration of titanium. The intensity of emission bands at 367 and 470 nm is lower for the samples calcined at 500 °C, compared to those calcined at 700 °C. This is because the number of oxygen vacancies on the surface increases on increasing the calcination temperature.

Figures 13b and 14b show the PL spectra of $Ti_xMg_{1-x}O$ samples, calcined at 500 and 700 °C, respectively, with an excitation wavelength of 500 nm, and Figs. 13c and 14c show the PL spectra of the same samples with an excitation wavelength of 550 nm. On excitation at 500 nm, pure MgO shows an emission band at about 753 nm and $Ti_xMg_{1-x}O$ samples, calcined at 500 and 700 °C, show emission bands at around 684 and 753 nm. Pure MgO as well as $Ti_xMg_{1-x}O$ samples calcined at 500 and 700 °C show an emission band at about 828 nm. The emission bands in the NIR region are attributed to capture and combination of charge carriers at the defect sites located within the band gap. These defects are associated with grains, orientation of crystallites, and thermal stress in the crystal (Ho and Huang 2013). The intensity of the NIR emission decreases in the $Ti_xMg_{1-x}O$ samples on increasing the concentration of titanium which is attributed to a decrease in the number of grain defects on increasing the concentration of titanium isopropoxide used during synthesis. On increasing the calcination temperature, the intensity of emission bands in NIR region increases because calcination at high temperature induces more thermal stress and increases defects associated with the grain boundaries (Ho and Huang 2013).

Materials with one-dimensional nanostructure exhibit good electron transport and photochemical activity (Yann et al. 2013). Although there are several methods reported for the synthesis of 1D structures (Wang et al. 2004; Jiang et al. 2012; Liu et al. 2011; Qu et al. 2010), in the case of magnesium titanate it is difficult to obtain 1D structure due to isotropic crystal

Table 6 Summary of PL emission bands for $Ti_xMg_{1-x}O$ samples calcined at 500 and 700 °C

Sl. no.	Sample ID	$\lambda_{excitation} = 250$ nm		$\lambda_{excitation} = 500$ nm		$\lambda_{excitation} = 550$ nm	
		500 °C (nm)	700 °C (nm)	500 °C (nm)	700 °C (nm)	500 °C (nm)	700 °C (nm)
1.	[Ti:Mg = 0.0:1.0]	367	369	753	753	828	828
2.	[Ti:Mg = 0.02:0.98]	367, 470	368, 470	683, 754	685, 753	828	828
3.	[Ti:Mg = 0.04:0.96]	367, 470	368, 470	684, 753	685, 753	828	828
4.	[Ti:Mg = 0.10:0.90]	368, 470	368, 470	684, 753	685, 753	828	828
5.	[Ti:Mg = 0.20:0.80]	368, 470	368, 470	684, 753	685, 753	828	828
6.	[Ti:Mg = 0.33:0.66]	368, 470	368, 470	684, 753	685, 753	828	828
7.	[Ti:Mg = 0.50:0.50]	368, 470	368, 470	684, 753	685, 753	828	828
8.	[Ti:Mg = 1.0:0.0]	373, 470	373, 470	753	753	828	828

structure of precursors for titanium (Yu et al. 2007). Semiconductors with band gap in the range 3.2–4.5 eV play an important role in various applications such as photocatalysis (Wang et al. 2004; Bandara et al. 2006, 2004), lithium-ion batteries (Jiang et al. 2012; Li et al. 2012), water splitting (Liu et al. 2011), dye-sensitized solar cells (Qu et al. 2010; Zhang et al. 2014; Cheng et al. 2013; Li et al. 2011; Jung et al. 2005), and dielectric materials (Tang et al. 2014; Xue et al. 2013). There are some reports on tuning the band gap of magnesium titanates from about 3.2 to 3.6 eV on varying the concentration of titanium and changing the calcination temperature (Bayal and Jeevanandam 2014; Ferri et al. 2009). The present study reports the synthesis of band gap-tunable Ti^{4+}-doped MgO heteronanostructures with a wide band gap range ($E_g = 3.2$ eV to 4.2 eV) with flower- and hexagonal rod-like morphology with a larger range of titanium concentration (0.02–0.50 mmol) for the first time by a facile thermal decomposition approach.

Conclusions

In the present study, $Ti_xMg_{1-x}O$ heteronanostructures ($x = 0.0$–0.50) have been synthesized by a novel thermal decomposition approach. Phase analysis of the precursors demonstrates the formation of Ti–Mg glycolates and $Ti_xMg_{1-x}O$ samples are formed by the solid-state decomposition of Ti–Mg glycolates at 500 and 700 °C. Phase analysis of the $Ti_xMg_{1-x}O$ samples calcined at 500 °C confirms the formation of MgO in the samples prepared using 0.02–0.10 mmol of titanium isopropoxide and amorphous phase in the

samples prepared using 0.20–0.50 mmol of titanium isopropoxide. After calcination at 700 °C, formation of MgO–$MgTiO_3$ is observed in the samples prepared using 0.02–0.10 mmol of titanium isopropoxide and pure $MgTiO_3$ is formed in the samples prepared using 0.20–0.50 mmol of titanium isopropoxide. Morphological studies by FE-SEM and TEM analysis confirm the formation of particles with rod- and flower-like morphology in the $Ti_xMg_{1-x}O$ samples. The optical band gap of $Ti_xMg_{1-x}O$ samples varies in a wide range (3.2–4.2 eV) as a function of titanium concentration and calcination temperature. In the photoluminescence spectra, emission bands at around 367 and 470 nm are observed due to surface oxygen vacancies and NIR emission bands observed at around 684, 753, and 828 nm are attributed to the defects located within the band gap. These heteronanostructures are expected to be useful in photocatalysis, dye-sensitized solar cells, and dielectric materials.

References

Bain S, Ma Z, Cui Z, Zhang L, Niu F, Song W (2008) Synthesis of micrometer-sized nanostructured magnesium oxide and its high catalytic activity in the Claisen-Schmidt

condensation reaction. J Phys Chem C 112:11340–11344. doi:10.1021/jp802863j

Bandara J, Hadapangoda CC, Jayasekera WG (2004) TiO₂/MgO composite photocatalyst: the role of MgO in photoinduced charge carrier separation. Appl Catal B 50:83–88. doi:10.1016/j.apcatb.2003.12.021

Bandara J, Kuruppu SS, Pradeep UW (2006) The promoting effect of MgO layer in sensitized photodegradation of colorants on TiO₂/MgO composite oxide. Colloids Surf A 276:197–202. doi:10.1016/j.colsurfa.2005.10.059

Bayal N, Jeevanandam P (2014) Synthesis of TiO₂–MgO mixed metal oxide nanoparticles via a sol gel method and studies on their optical properties. Ceram Int 40:15463–15477. doi:10.1016/j.ceramint.2014.06.122

Bian S, Baltrusaitis J, Galhotra P, Grassian VH (2010) A template-free, thermal decomposition method to synthesize mesoporous MgO with a nanocrystalline framework and its application in carbon dioxide adsorption. J Mater Chem 20:8705–8710. doi:10.1039/c0jm01261k

Bokhimi X, Boldu JL, Munoz E Novaro O (1999) Structure and composition of the nanocrystalline phases in a MgO-TiO₂ system prepared via sol-gel technique. Chem Mater 11:2716–2721. doi:10.1021/cm9900812

Cao AM, Hu JS, Liang HP, Song WG, Wan LJ, He XL, Gao XG, Xia SH (2006) Hierarchically structured cobalt oxide (Co₃O₄): the morphology control and its potential in sensors. J Phys Chem B 110:15858–15863. doi:10.1021/jp0632438

Ceylantekin R, Aksel C (2012) Improvements on the mechanical properties and thermal shock behaviours of MgO-spinel composite refractories by ZrO₂ incorporation. Ceram Int 38:995–1002. doi:10.1016/j.ceramint.2011.08.022

Chakroune N, Viau G, Ammar S, Jouini N, Gredin P, Vaulaya MJ, Fieveta F (2005) Synthesis, characterization and magnetic properties of disk-shaped particles of a cobalt alkoxide: Co^{II}(C₂H₄O₂). New J Chem 29:355–361. doi:10.1039/b411117f

Cheng G, Akhtar MS, Yang OB, Stadlera FJ (2013) Structure modification of anatase TiO₂ nanomaterials-based photoanodes for efficient dye-sensitized solar cells. Electrochim Acta 113:527–535. doi:10.1016/j.electacta.2013.09.085

Dadvar S, Tavanai H, Morshed M, Ghiaci M (2013) A study on the kinetics of 2-chloroethyl ethyl sulfide adsorption onto nanocomposite activated carbon nanofibers containing metal oxide nanoparticles. Sep Purif Technol 114:24–30. doi:10.1016/j.seppur.2013.04.019

Devaraja PB, Avadhani DN, Prashantha SC, Nagabhushana H, Sharma SC, Nagabhushana BM, Nagaswarupa HP (2014) Synthesis, structural and luminescence studies of magnesium oxide nanopowder. Spectrochim Acta Part A 118:847–851. doi:10.1016/j.saa.2013.08.050

Dong W et al (2011) General approach to well-defined perovskite MTiO₃ (M = Ba, Sr, Ca, and Mg) nanostructures. J Phys Chem C 115:3918–3925. doi:10.1021/jp110660v

Ferri EAV et al (2009) Photoluminescence behavior in MgTiO₃ powders with vacancy/distorted clusters and octahedral tilting. Mater Chem Phys 117:192–198. doi:10.1016/j.matchemphys.2009.05.042

Fujiokaa Y, Frantti J, Nieminen RM (2012) Ferromagnetism in MgTiO₃–Ti₂O₃ solid solutions. Mater Sci Forum 700:23–27. doi:10.4028/www.scientific.net/MSF.700.23

FujiokaY Frantti J, Nieminen RM (2011) Itinerant-electron ferromagnetism in a titanium-rich magnesium titanate ilmenite solid solution. J Phys Chem C 115:1457–1463. doi:10.1021/jp107698j

Gao L, Zhai J, Yao X (2008) MgTiO₃ and Ba₀.₆₀Sr₀.₄₀Mg₀.₁₅Ti₀.₈₅O₃ composite thin films with promising dielectric properties for tunable applications. J Am Ceram Soc 91:3109–3112. doi:10.1111/j.1551-2916.2008.02569.x

Gao DZ, Watkins MB, Shluger AL (2012) Transient mobility mechanisms of deposited metal atoms on insulating surfaces: Pd on MgO (100). J Phys Chem C 116:14471–14479. doi:10.1021/jp303951y

Ho YD, Huang CL (2013) Strong near-infrared photoluminescence emission of (003)-oriented MgTiO₃ thin films. J Am Ceram Soc 96:2065–2068. doi:10.1111/jace.12439

Ho YD, Su CH, Huang CL (2014) Intense red photoluminescence emission of sol–gel-derived nanocrystalline Mg₂TiO₄ thin films. J Am Ceram Soc 97:358–360. doi:10.1111/jace.12775

Huang CL, Liu SS, Chen SH (2011) The effect of non-stoichiometry on the microstructure and microwave dielectric properties of the Mg₁₊ₓTiO₃₊ₓ ceramics. J Alloys Compd 509:9702–9707. doi:10.1016/j.jallcom.2011.07.092

Jiang X, Herricks T, Xia Y (2003) Monodispersed spherical colloids of titania: synthesis, characterization and crystallization. Adv Mater 15:1205–1209. doi:10.1002/adma.200305105

Jiang X, Wang Y, Herricks T, Xia Y (2004) Ethylene glycol-mediated synthesis of metal oxide nanowires. J Mater Chem 14:695–703. doi:10.1039/b313938g

Jiang Y, Wang K, Guo X, Wei X, Wang J, Chen J (2012) Mesoporous titania rods as an anode material for high performance lithium-ion batteries. J Power Sources 214:298–302. doi:10.1016/j.jpowsour.2012.04.091

Jung HS, Lee JK, Nastasi M (2005) Preparation of nanoporous MgO-coated TiO₂ nanoparticles and their application to the electrode of dye-sensitized solar cells. Langmuir 21:10332–10335. doi:10.1021/la051807d

Lee JW, Ko JH (2014) Defect states of transition metal-doped MgO for secondary electron emission of plasma display panel. J Inf Disp 15:157–161. doi:10.1080/15980316.2014.955140

Li S, Shena Q, Zong J, Yang H (2010) Simple preparation of sub-micron mesoporous TiO₂ spheres consisting of anatase nanocrystals. J Alloys Compd 508:99–105. doi:10.1016/j.jallcom.2010.04.246

Li L, Yang X, Gao J, Zhao J, Hagfeldt A, Sun L (2011) Electric characteristics of MgO-doped TiO₂ nanocrystalline film in dye-sensitized solar cells. Adv Mater Res 236:2106–2109. doi:10.4028/www.scientific.net/AMR.236-238.2106

Li C, Li Q, Chen L, Wang T (2012) A facile titanium glycolate precursor route to mesoporous Au/Li₄Ti₅O₁₂ spheres for high-rate lithium-ion batteries. ACS Appl Mater Interfaces 4:1233–1238. doi:10.1021/am2018145

Liu M, Snapp NL, Park H (2011) Water photolysis with a cross-linked titanium dioxide nanowire anode. Chem Sci 2:80–87. doi:10.1039/c0sc00321b

Mohammadi MR, Fray DJ (2012) Tailoring of morphology and crystal structure of nanomaterials in MgO–TiO$_2$ system by controlling Mg:Ti molar ratio. J Sol-Gel Sci Technol 64:135–144. doi:10.1007/s10971-012-2839-y

Pfaff G (1994) Peroxide route for synthesis of magnesium titanate powders of various compositions. Ceram Int 20:111–116. doi:10.1016/0272-8842(94)90067-1

Pol VG, Langzam Y, Zaban A (2007) Application of microwave superheating for the synthesis of TiO$_2$ rods. Langmuir 23:11211–11216. doi:10.1021/la7020116

Qu Y, Zhou W, Pan K, Tian C, Ren Z, Dong Y, Fu H (2010) Hierarchical anatase TiO$_2$ porous nanopillars with high crystallinity and controlled length: an effective candidate for dye-sensitized solar-cells. Phys Chem Chem Phys 12:9205–9212. doi:10.1039/b922658c

Qu Y et al (2012) Facile preparation of porous NiTiO$_3$ nanorods with enhanced visible-light-driven photocatalytic performance. J Mater Chem 22:16471–16476. doi:10.1039/c2jm32044d

Qu Y et al (2013) A novel phase-mixed MgTiO$_3$–MgTi$_2$O$_5$ heterogeneous nanorod for high efficiency photocatalytic hydrogen production. Chem Commun 49:8510–8512. doi:10.1039/c3cc43435d

Rao Y, Wang W, Tan F, Cai Y, Lu J, Qiao X (2013) Influence of different ions doping on the antibacterial properties of MgO nanopowders. Appl Surf Sci 284:726–731. doi:10.1016/j.apsusc.2013.08.001

Shrestha KM, Sorensen CM, Klabunde KJ (2013) MgO–TiO$_2$ mixed oxide nanoparticles: comparison of flame synthesis versus aerogel method; characterization, and photocatalytic activities. J Mater Res 28:431–439. doi:10.1557/jmr.2012.288

Subramania A, Kumar GV, Priya ARS, Vasudevan T (2007) Polyol-mediated thermolysis process for the synthesis of MgO nanoparticles and nanowires. Nanotechnology. doi:10.1088/0957-4484/18/22/225601

Tang B, Li H, Fan P, Yu S, Zhang S (2014) The effect of Mg:Ti ratio on the phase composition and microwave dielectric properties of MgTiO$_3$ ceramics prepared by one synthetic process. J Mater Sci Mater Electron 25:2482–2486. doi:10.1007/s10854-014-1899-x

Tian P, Han X, Ning G, Fang H, Ye J, Gong W, Lin Y (2013) Synthesis of porous hierarchical MgO and its superb adsorption properties. ACS Appl Mater Interfaces 5:12411–12418. doi:10.1021/am403352y

Wang D, Yu D, Chen Y, Kumada N, Kinomura N, Takano M (2004) Photocatalysis property of needle-like TiO$_2$ prepared from a novel titanium glycolate precursor. Solid State Ionics 172:101–104. doi:10.1016/j.ssi.2004.04.028

Wang W, Qiao X, Chen J, Tan F (2008) Preparation and characterization of Ti-doped MgO nanopowders by a modified coprecipitation method. J Alloys Compd 461:542–546. doi:10.1016/j.jallcom.2007.07.046

Wang W, Qiao X, Chen J, Tan F, Li H (2009) Influence of titanium doping on the structure and morphology of MgO prepared by coprecipitation method. Mater Charact 60:858–862. doi:10.1016/j.matchar.2009.02.002

Wang X, Cai J, Zhang Y, Li L, Jiang L, Wang C (2015) Heavy metal sorption properties of magnesium titanate mesoporous nanorods. J Mater Chem A 3:11796–11800. doi:10.1039/c5ta02034d

Xue X, Yu H, Xu G (2013) Phase composition and microwave dielectric properties of Mg-excess MgTiO$_3$ ceramics. J Mater Sci Mater Electron 24:1287–1291. doi:10.1007/s10854-012-0921-4

Yadav MK, Kothari AV, Gupta VK (2011) Preparation and characterization of bi- and trimetallic titanium based oxides. Dyes Pigm 89:149–154. doi:10.1016/j.dyepig.2010.10.004

Yang KC, Shen P (2005) On the precipitation of coherent spinel nanoparticles in Ti-doped MgO. J Solid State Chem 178:661–670. doi:10.1016/j.jssc.2004.12.019

Yann LD, Gilles A, Mihai S, Rouessac V, Tingry S, Barboiu M (2013) Dynamic constitutional electrodes toward functional fullerene wires. Chem Commun 49:3667–3669. doi:10.1039/c3cc41450g

Yu HK, Eun TH, Yi GR, Yang SM (2007) Multi-faceted titanium glycolate and titania structures from room-temperature polyol process. J Colloid Interface Sci 316:175–182. doi:10.1016/j.jcis.2007.07.043

Zhang Y et al (2014) Mesoporous titanium oxide microspheres for high-efficient cadmium sulfide quantum dot-sensitized solar cell and investigation of its photovoltaic behavior. Electrochim Acta 150:167–172. doi:10.1016/j.electacta.2014.10.101